Supplementary Fig. 1-11

Inhibitors for a conserved filarial catechol-*O*-methyltransferase possess *in vivo* curative potency against *Brugia malayi* infection

Supplementary Fig. 1. Computational workflow for protein ternary complex modeling and molecular dynamics (MD) analysis. **Step 1**: The BmMT structure (AF-A0A0K0JDP8-F1) is predicted using AlphaFold. The Predicted Local Distance Difference Test (pLDDT) is a per-residue confidence metric (0–100) used by AlphaFold to assess how well a predicted structure matches an experimental structure. High pLDDT (>70–90) indicates high confidence in local atomic placement, while low pLDDT (<50) often signals intrinsically disordered regions (IDRs). The structure was refined via all-atom MD simulation in an explicit water box with Na^+ and Cl^- counterions; backbone root-mean-square deviation (RMSD) over time indicates structural equilibration across triplicate runs. **Step 2**: RMSD-based clustering of the MD trajectory identifies dominant conformational states (e.g., Cluster 1 at 73%), and the representative structure from clustering was superimposed onto human COMT (RMSD ~ 3 Å) to transfer the coordinates of S-adenosylmethionine (SAM), magnesium ion (Mg2+), and 3,5-dinitrocatechol (DNC) into the BmMT structure; this ternary structure was then used as the receptor (with SAM and Mg2+ included as part of the receptor) for induced-fit flexible docking of BmMT inhibitors. **Step 3**: The ternary complex is simulated to evaluate stability and protein-ligand interactions through MD trajectory analysis.

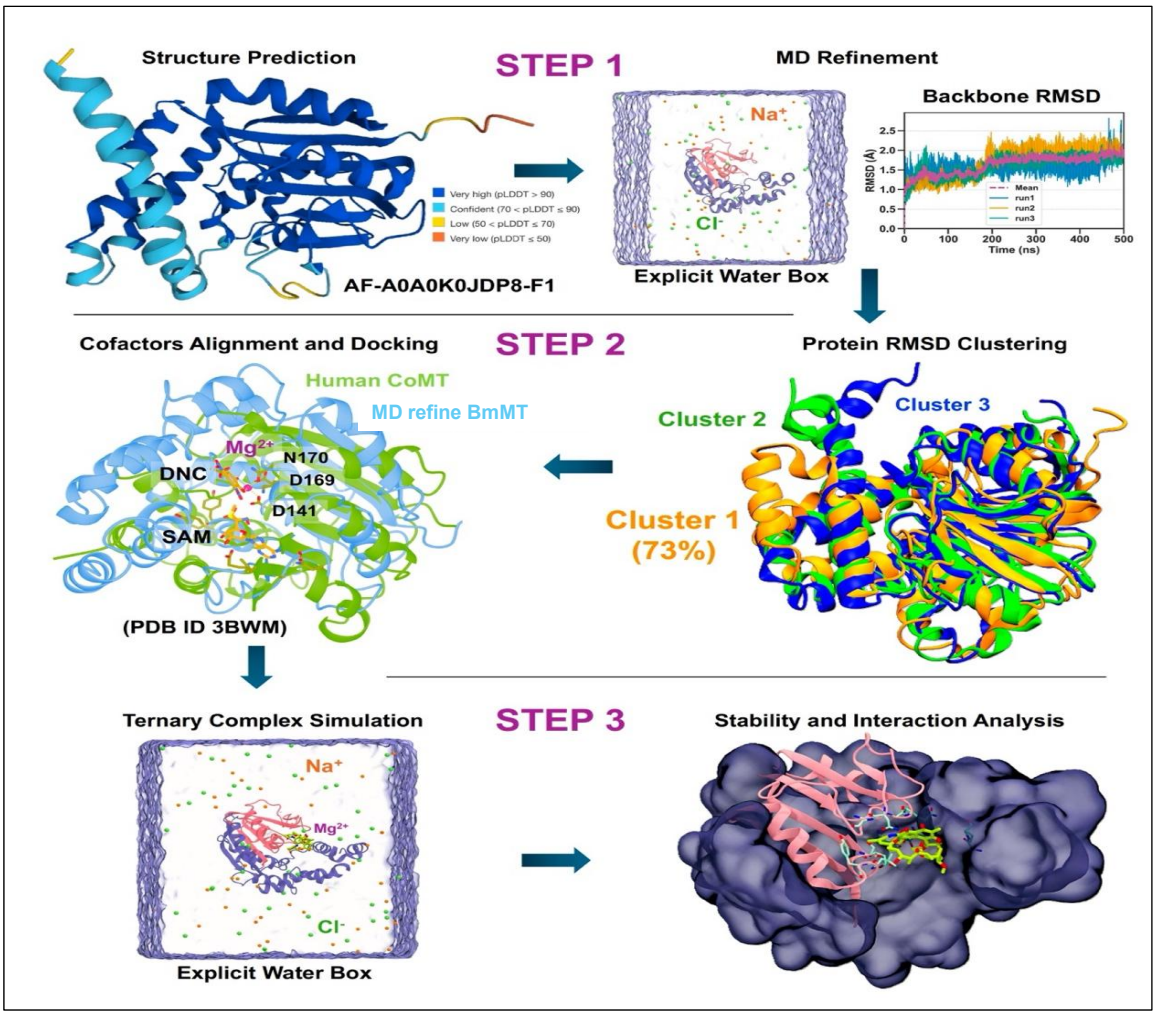

Supplementary Fig. 2. Analysis of MTase-Glo detection interference by BmMT inhibitors. Four reconstituted BmMT inhibitors were tested at a final concentration of 50 µM for the MTase-Glo detection interference assay. Compounds were incubated with 1 µM of S-adenosylhomocysteine (SAH) in a 50 µL reaction. The SAH-only control group contained 1 µM SAH and 1% DMSO volume equivalent to that used for inhibitors. Relative luminescence units (RLU) were background-corrected using wells containing reaction buffer and DMSO only. All assays were performed in triplicate, and data are presented as mean ± SEM from three independent experiments

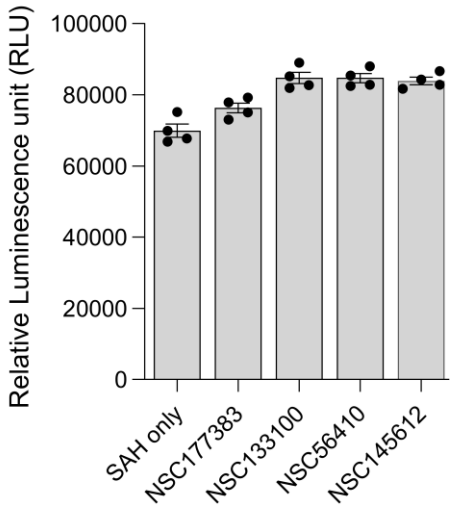

Supplementary Fig. 3. Analysis of the effects of BmMT inhibitors on *B. malayi* L3 larvae survival *in vitro*. *B. malayi* L3 larvae were treated with 50 µM of ivermectin, BmMT inhibitor (NSC177383, NSC145612, NSC65410, or NSC133100) or 1% DMSO (compound solvent control) in culture. Worm survival % was determined as the percent of completely immotile larvae out of 10 L3 larvae in triplicate cultures, and was normalized to the cultures treated with DMSO. The data are presented as mean ± SEM from three independent experiments.

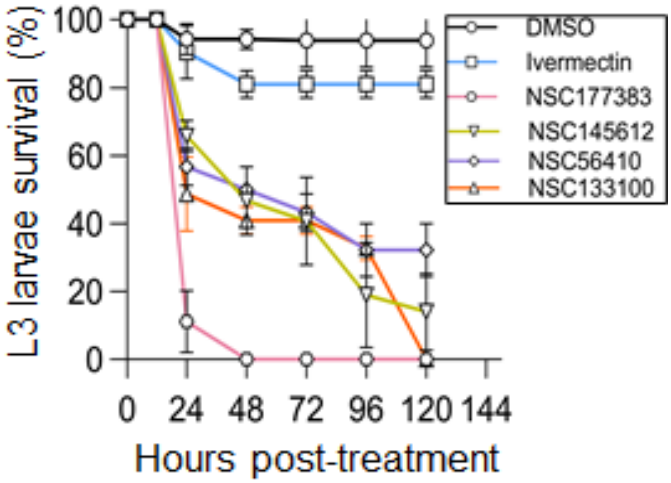

Supplementary Fig. 4. Catecholamines ELISA quantification standard curve. Two-fold serially diluted standard catecholamines solutions (240, 120, 60, 30, and 15 pg/mL) were used to generate the quantification standard curve. Absorbance was measured at 450 nm and background- corrected absorbance (minus absorbance from blank wells) values were plotted against corresponding catecholamine concentrations, and a linear regression line was fitted in the GraphPad Prism v10. Data was interpolated from the equation derived from the linear regression.

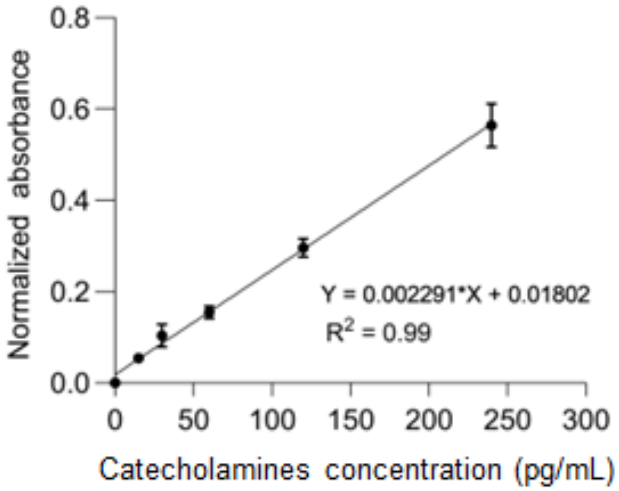

Supplementary Fig. 5. Protein backbone RMSD across six BmMT simulation systems. RMSD of protein backbone heavy atoms (Cα, C, N) relative to the minimized starting structure for Apo+Mg (blue), the DNC reference complex (black), and the four BmMT inhibitors: NSC56410 (orange), NSC177383 (light blue), NSC133100 (green), and NSC145612 (pink). In each time-series, the bold line is the across-replica mean, and the shaded band is ±1 SD; faint traces show the three individual 500 ns replicas. The narrow strip on the right of each panel is the Gaussian kernel density estimate (bandwidth = 0.15) of the pooled RMSD distribution over the three replicas. The mean ± standard deviation (SD) value reported inside each panel is computed over the equilibrated window (last 300 ns, all replicas pooled): Apo+Mg 1.56 ± 0.20 Å, Reference (DNC) 1.68 ± 0.32 Å, NSC56410 1.94 ± 0.15 Å, NSC177383 1.70 ± 0.21 Å, NSC133100 1.71 ± 0.26 Å, and NSC145612 1.69 ± 0.19 Å. All ligand-bound systems equilibrate within ~100 ns and remain within ~0.4 Å of the Apo+Mg baseline, indicating that none of the candidate ligands induces large-scale backbone rearrangement of the BmMT scaffold. NSC56410 shows the highest mean RMSD (1.94 Å) but the tightest distribution (SD 0.15 Å), consistent with a stable but slightly shifted backbone conformation rather than progressive drift. All simulations were run in triplicate (n = 3 × 500 ns, total 1.5 μs per system); smoothed traces represent a 1 ns rolling mean.

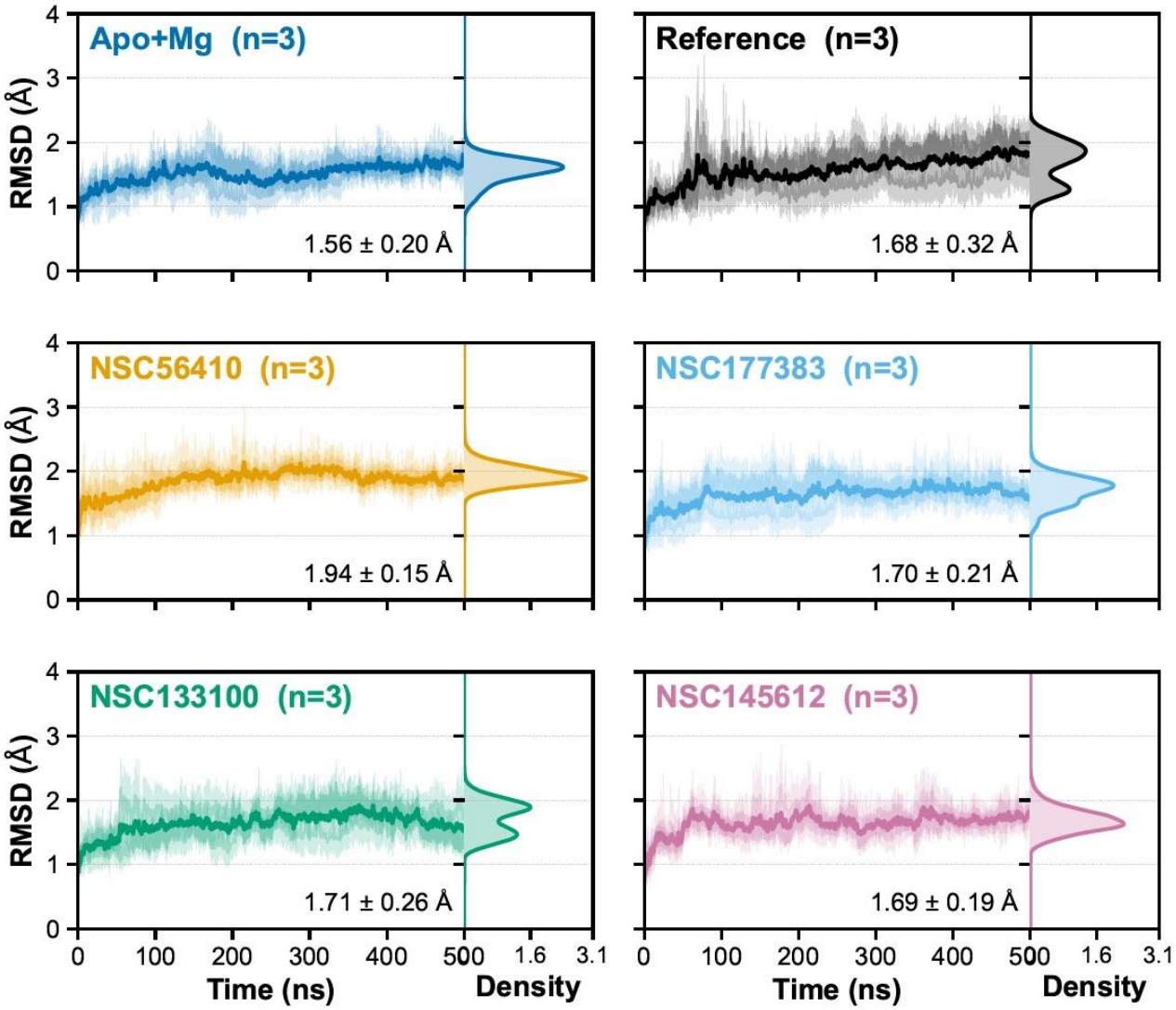

Supplementary Fig. 6. Radius of gyration (R_g) of the protein backbone (Cα, C, N) as a measure of overall compactness for Apo+Mg (blue), the DNC reference complex (black), and the four NSC ligand-bound systems: NSC56410 (orange), NSC177383 (light blue), NSC133100 (green), and NSC145612 (pink). In each time-series the bold line is the across-replica mean and the shaded band is ±1 SD; faint traces show the three individual 500-ns replicas. The narrow strip on the right of each panel is the Gaussian kernel density estimate (bandwidth = 0.15) of the pooled R_g distribution over the three replicas. The mean ± SD value reported inside each panel is computed over the equilibrated window (last 300 ns, all replicas pooled): Apo+Mg 17.83 ± 0.14 Å, Reference 17.87 ± 0.15 Å, NSC56410 18.11 ± 0.15 Å, NSC177383 18.13 ± 0.13 Å, NSC133100 18.21 ± 0.12 Å, and NSC145612 18.12 ± 0.14 Å. All ligand-bound systems show a small, systematic R_g expansion of ~0.25–0.35 Å relative to Apo+Mg (17.83 Å) and the DNC reference (17.87 Å), consistent with ligand occupancy of the substrate pocket producing a modestly larger but tightly distributed conformation; NSC133100 shows the largest shift (+0.38 Å), while NSC145612 and NSC177383 track closest to the reference. The narrow SDs (≤0.15 Å across all systems) and unimodal density profiles indicate that each trajectory samples a single, well-defined compactness state with no evidence of domain opening or partial unfolding. All simulations were run in triplicate (n = 3 × 500 ns, total 1.5 µs per system); smoothed traces represent a 1 ns rolling mean.

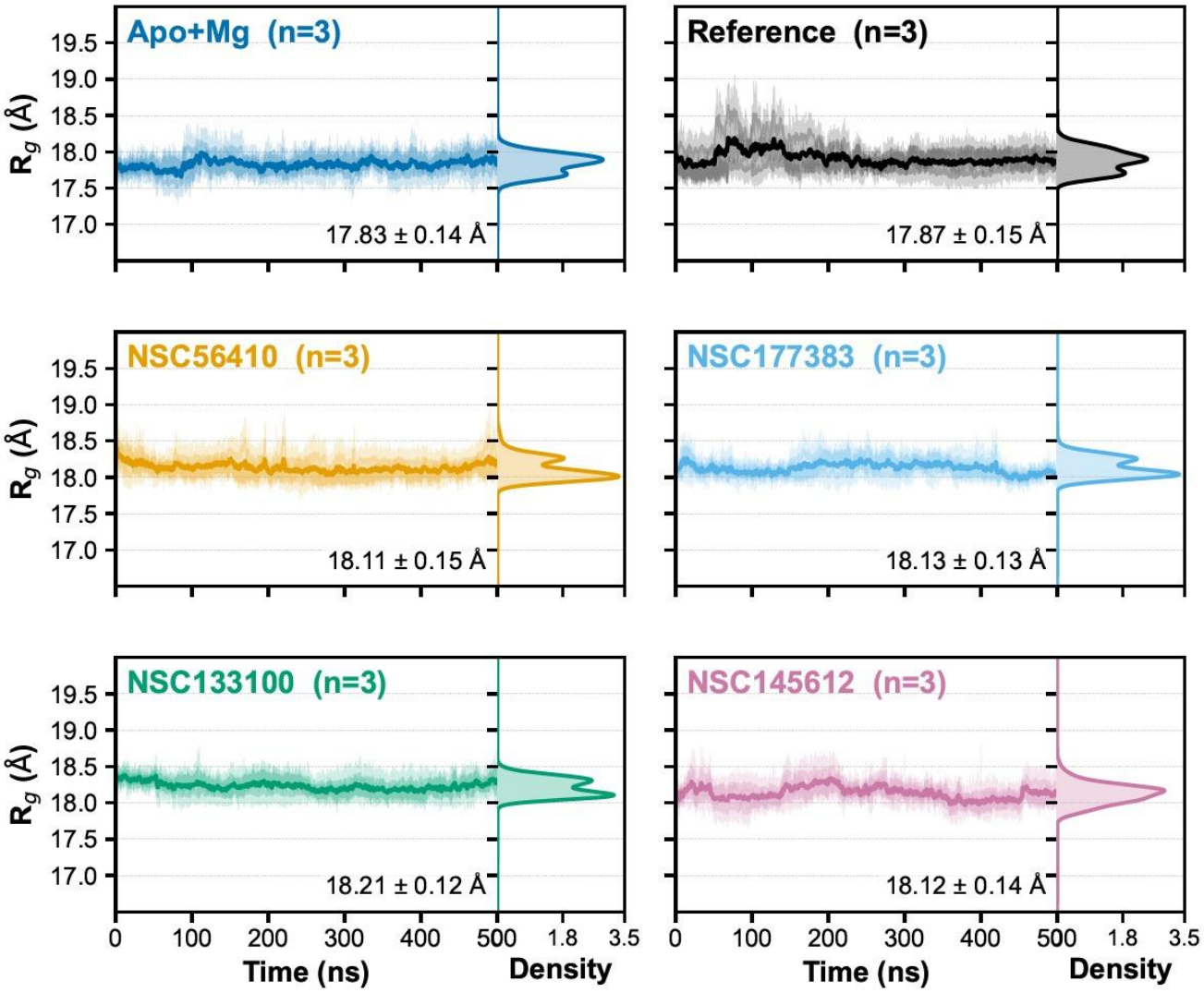

Supplementary Fig. 7. Solvent-accessible surface area (SASA) of SAM and bound ligands across the BmMT simulation systems. SASA (Å²) of the cofactor SAM and of each bound small-molecule ligand computed over the full 500 ns production trajectory for the DNC reference complex (black) and the ligand-bound systems: NSC56410 (orange), NSC177383 (light blue), NSC133100 (green), and NSC145612 (pink). In each time-series, the bold line is the across-replica mean, and the shaded band is ±1 SD; faint traces show the three individual 500-ns replicas. The narrow strip on the right of each panel is the Gaussian kernel density estimate of the pooled SASA distribution over the three replicas. The mean ± SD value reported inside each panel is computed over the equilibrated window (last 300 ns, all replicas pooled). Low and tightly distributed SASA values indicate that SAM and the ligands remain deeply buried in the active-site pocket throughout the simulations, with no evidence of partial dissociation or solvent exposure events. All simulations were run in triplicate (n = 3 × 500 ns, total 1.5 µs per system); smoothed traces represent a 1-ns rolling mean.

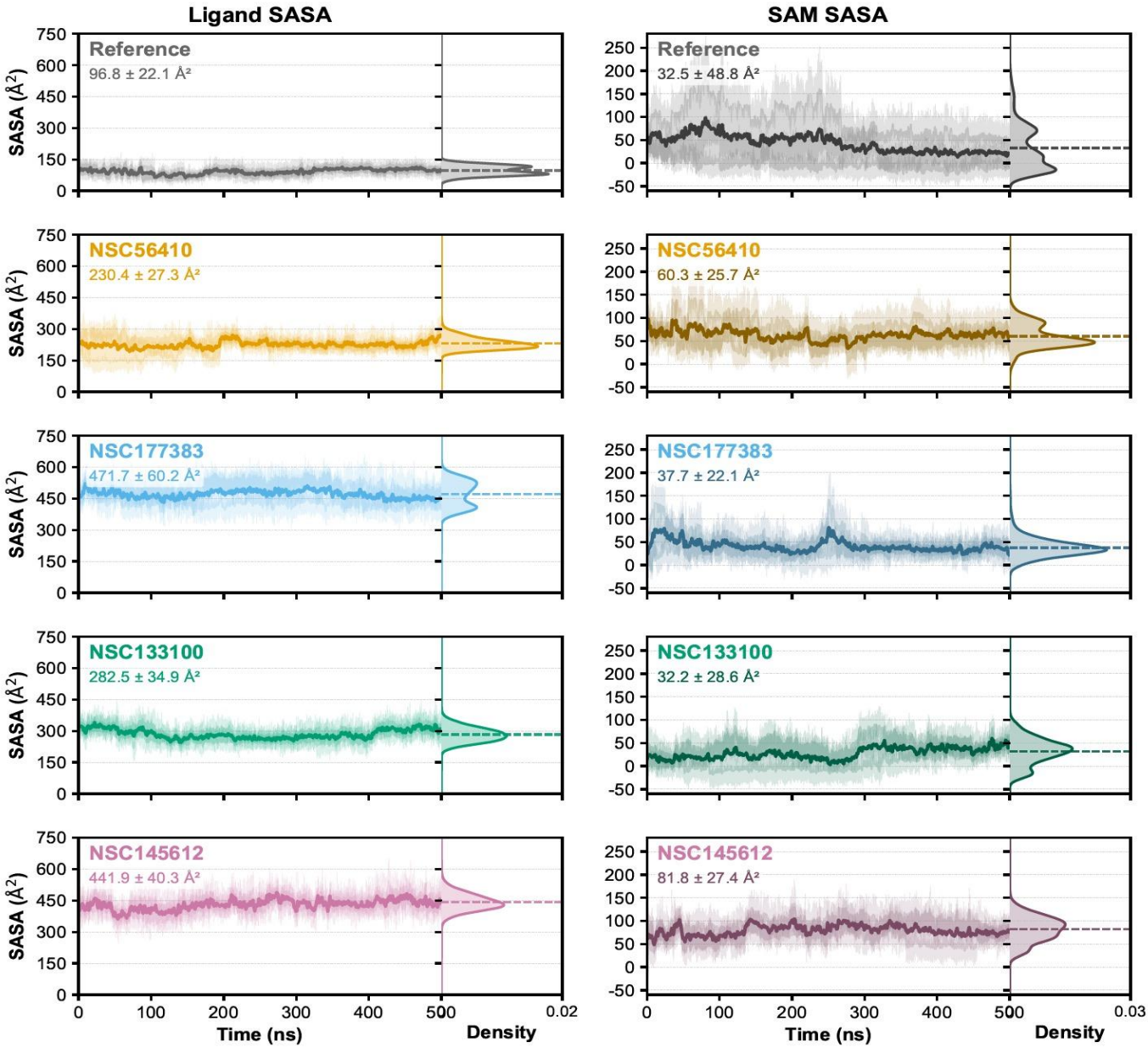

Supplementary Fig. 8. Ligand and SAM heavy-atoms RMSD relative to the minimized starting structure for Apo+Mg DNC (reference) and the ligand-bound systems (NSC56410, NSC177383, NSC133100, NSC145612). Each time series shows the replica mean (bold line) ± SD (shaded band) across three independent 500-ns MD simulations. The right panel shows the probability density (KDE) of the RMSD distribution over all replicas. Mean ± SD values (dotted lines) are indicated in each panel (for last 300 ns trajectory). Stable, low RMSD values for the ligand and SAM indicate a well-accommodated binding pose within the BmMT active site, while elevated or fluctuating ligand RMSD suggests instability or displacement from the binding pocket. Smoothed traces represent a 1 ns rolling mean. Probability densities were estimated using Gaussian kernel density estimation (bandwidth = 0.15).

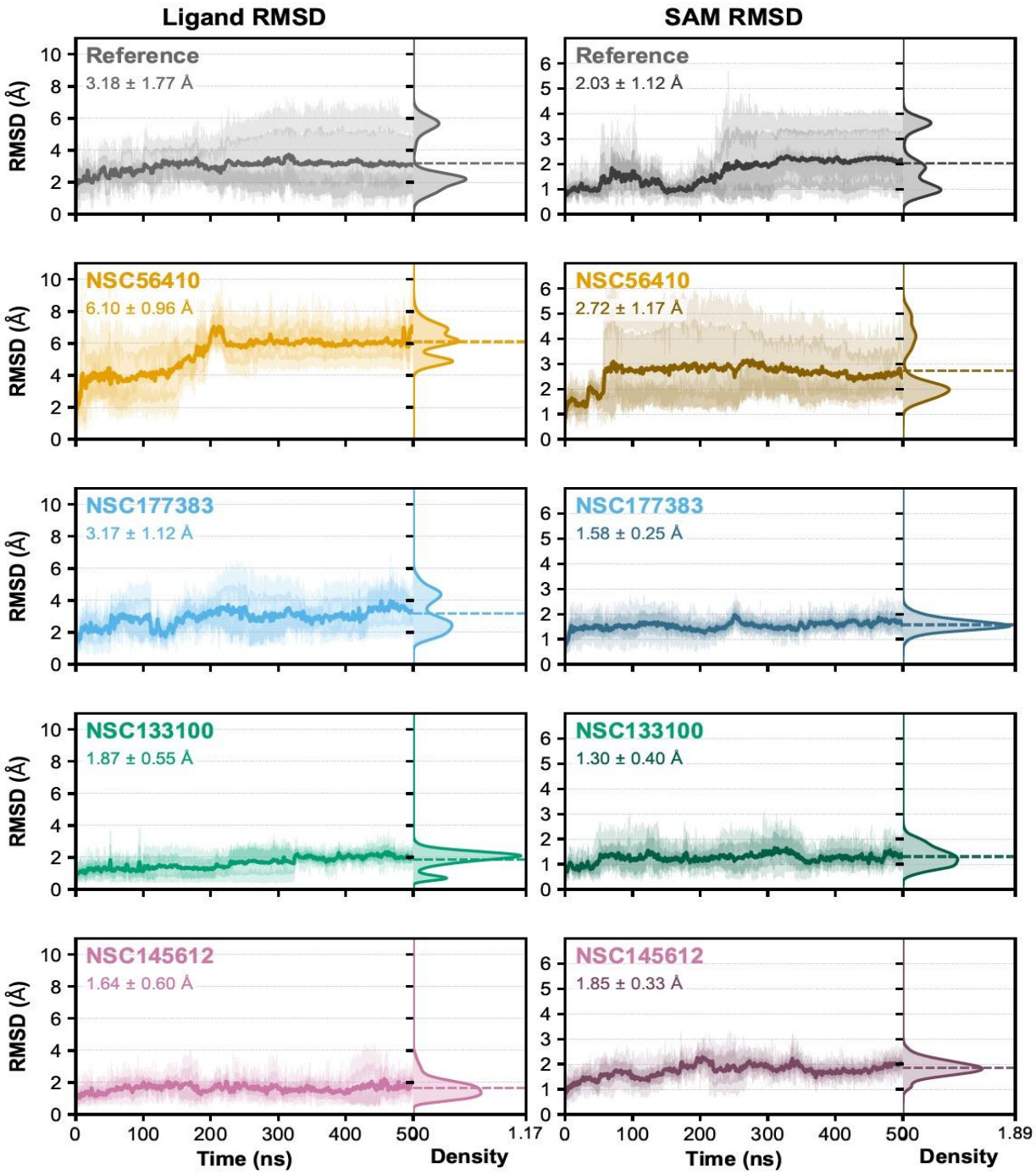

Supplementary Fig. 9. Ligand-binding pose cluster populations from VMD clustering. Stacked bar charts showing the distribution of binding pose clusters for each system, derived from the VMD-clustering plugin (num = 5) of the 500 ns trajectory with stride of 100 frames (1,500 frames, 3 replicas, RMSD cutoff 2.5 Å). DNC, NSC133100 and NSC145612 adopt a single dominant pose predominantly (Cluster 0: 75%, 76% and 88%, respectively), while NSC177383 shows moderate pose diversity (Cluster 0: 60%) and NSC56410 exhibits the highest heterogeneity, with Cluster 0 representing only 31% of frames alongside substantial contributions from Clusters 1 (19%) and 2 (19%).

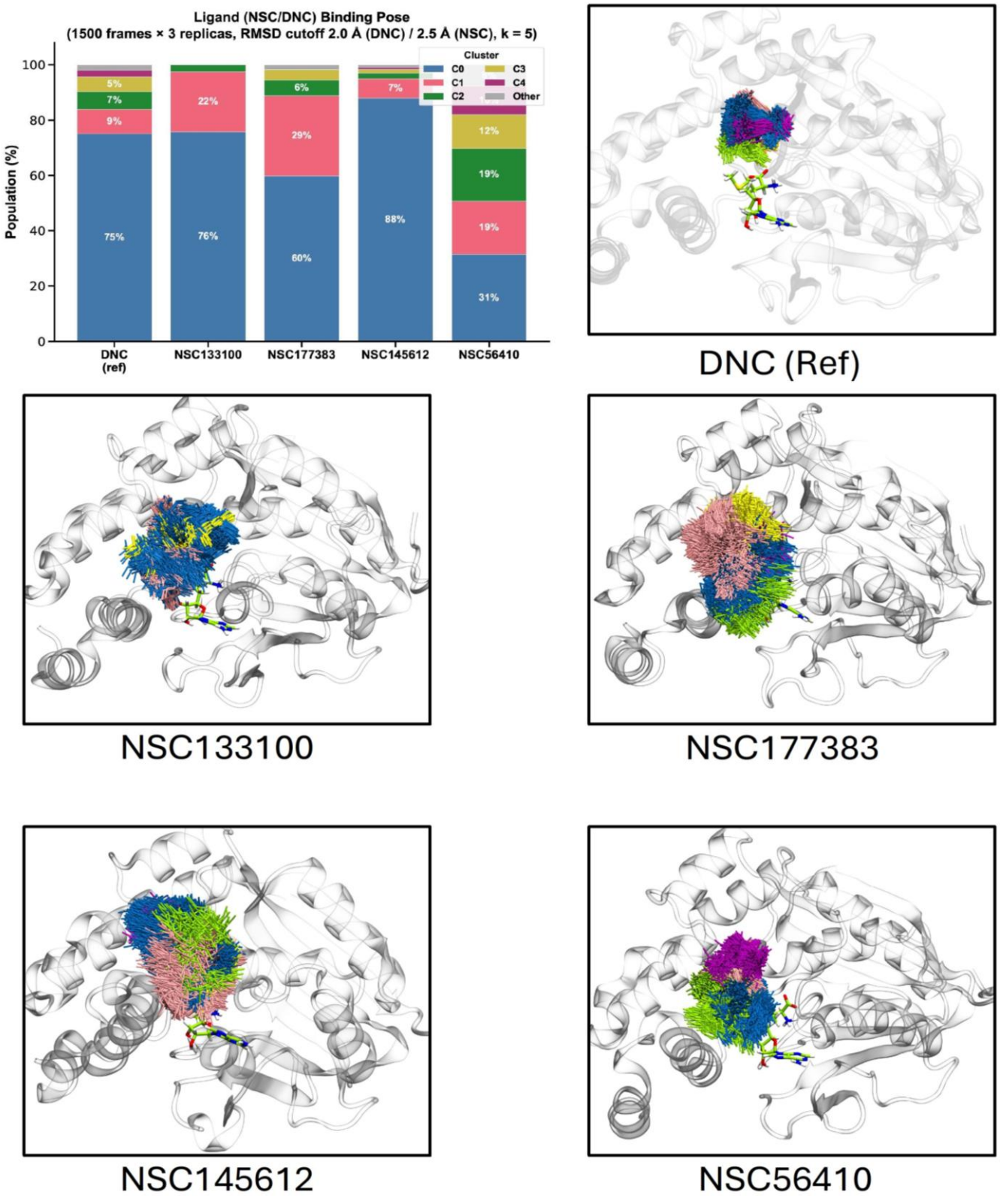

Supplementary Fig. 10. Predicted binding modes of candidate inhibitors in the SAM-dependent methyltransferase active site. **(a)** Heatmaps of Mg^{2+}–protein, Mg^{2+}–ligand, and SAM(CE)–ligand distances (Å) for the reference and the compounds. **(b)** Mean waters in the Mg^{2+} first hydration shell. (C–F) Active-site poses of NSC133100 **(c)**, NSC177383 **(d)**, NSC56410 **(e)**, and NSC145612 **(f)**, with ligand (orange), SAM (olive), Mg^{2+} (green sphere), waters (WAT), and key residues including E148, D177, and H151.

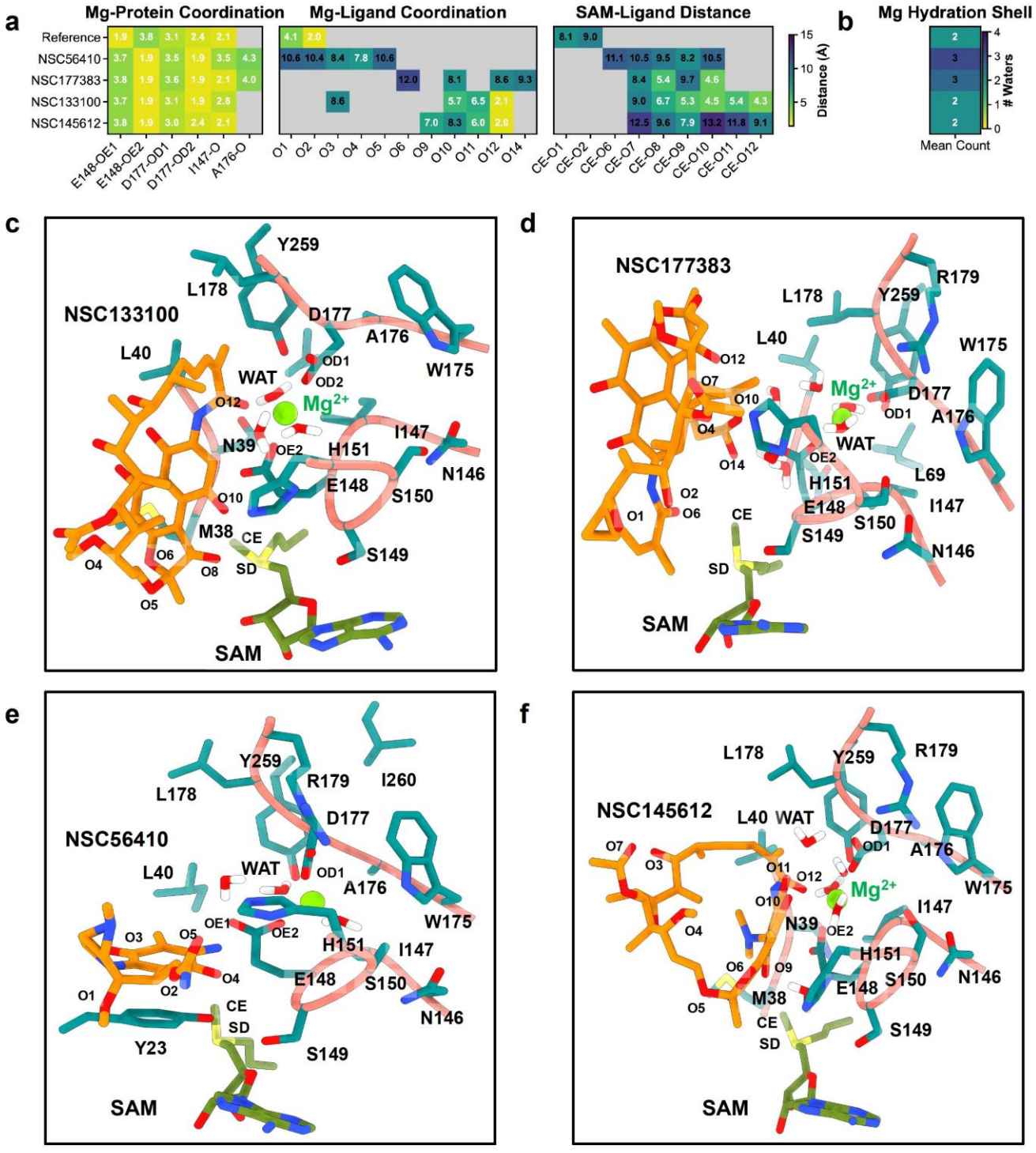

Supplementary Fig. 11. Hydrogen-bond analysis of the reference ligand DNC and the ligand bound to the BmMT. **(a–e)** Per-system hydrogen-bond occupancy (mean ± SD. across replicas, last 200 ns of MD) for all donor–acceptor pairs with ≥20% occupancy, labeled as donor–acceptor (ligand atoms prefixed LIG275; SAM cofactor prefixed SAM276): **(a)** DNC reference, dominated by a near-saturating LIG:O1–E148:OE1 contact (~90%) together with LIG:O1–E148:CD (~80%), LIG:O1–E148:OE2 (~55%), and LIG:O1–T240:O (~40%), a compact, carboxylate-anchored interaction pattern. **(b)** NSC133100, with a single dominant LIG:O10–H151:CE1 contact (~65%) and weaker secondary bonds to S248:OG, H151:NE2, and T240:OG1 (each ~20–30%). **(c)** NSC145612, engaging a dense H-bond network: saturating contacts with T240:OG1 (O2, O3) and the E148 carboxylate (OE1/OE2/CD) via ligand O11 and N1, plus auxiliary bonds to S248:OG**. (d)** NSC177383, showing the most diverse residue set, persistent contacts with R19 (N1–R19:O ~100%; R19:NH1–O7/C20/C40), H151 (CB/CA/NE2), T240:OG1, Y23:OH, N27:OD1, E148:OE1, Y219:OH, and D18:O. **(e)** NSC56410, anchored by LIG:N1–Y23:OH (~100%) and LIG:N3–M38:O (~95%), together with H151:NE2–O5, E148:OE1/CD, and direct SAM276:N6→LIG (N2/O1/C6) hydrogen bonds, the only system with significant direct SAM–ligand H-bonding. **(f)** Number of unique hydrogen bonds per system (≥10% occupancy, mean across replicas): DNC = 6, NSC133100 = 11, NSC145612 = 33, NSC177383 = 27, NSC56410 = 25. All four candidates form substantially more unique H-bonds than the DNC reference, with NSC145612 showing the largest and most stable H-bond network and NSC56410 uniquely bridging the substrate pocket to the SAM co-factor.